Journal of Applied Sciences

ISSN 1812-5654

science alert

ANSInet
an open access publisher
http://ansinet.com

Journal of Applied Sciences 8 (22): 4004-4016, 2008
ISSN 1812-5654

Using ETM+ and Airborne Geophysics Data to Locating Porphyry Copper and Epithermal Gold Deposits in Eastern Iran

[1,2]M.H. Karimpour, [1]A. Malekzadeh Shafaroudi, [2]C.R. Stern and [1]M.R. Hidarian
[1]Research Center for Ore Deposit of Eastern Iran, Ferdowsi University of Mashhad, P.O. Box 91775-1436, Mashhad, Iran
[2]Department of Geological Sciences, University of Colorado, CB-399, Boulder

Abstract: Enhanced Thematic Mapper Plus (ETM+) and airborne geophysics data have been used for locating porphyry copper and epithermal gold prospect areas related to hydrothermal alteration zones in the Lut block of eastern Iran. The Lut block has a great potential for different types of mineralization due to its extensive exposure of Cenozoic volcanic and subvolcanic calc-alkaline rocks generated in a subduction zone tectonic setting. Various ETM+ images processing techniques were employed, including false color composite images, color composite ratio images, standard PC image analysis on six bands and color composite selective PC images. Application of these techniques detected four major prospect areas and also identified another small previously unknown alteration area in the southeastern part of the district. Color composition selective PC images proved to be the most reliable method for exploration. Airborne magnetometry data show high magnetism over the most of the study area, resulting from the presence of magnetic-series granitoid rocks and/or propylitic/potassic alteration zones with magnetite veins related to mineralization. Low magnetic areas reflect intense magnetic destruction in other types of alteration zone. Radiometry detected areas of high K and U counts that have resulted from the presence of sericite, clay minerals and K-feldspar in alteration zones with low magnetism.

Key words: Lut block, landsat, image processing, magnetometry, radiometry

INTRODUCTION

Remote sensing can be used to recognize altered rocks because their reflectance spectra differ from those of the unaltered rocks (Sabins, 1999). Hydroxyl-bearing minerals (in sericite, argillic and alunitic zones) and iron oxides (in gossan zone) can be detected by remote sensing techniques. ETM+, ASTER, SPOT and AVIRIS data have been widely used for mineral exploration associated with hydrothermal alteration (Abrams *et al*., 1977, 1983; Buckingham and Sommer, 1983; Goetz *et al*., 1983; Conradsen and Harpoth, 1984; Amos and Greenbaum, 1989; Drury and Hunt, 1989; Swayze *et al*., 1998; Ramadan *et al*., 2001; Rowan *et al*., 2003; Ranjbar *et al*., 2004; Chen *et al*., 2007). Porphyry copper and epithermal gold deposits can be clearly enhanced by remote sensing methods due to extensive hydrothermal alteration such as potassic, sericitic, silicification, argillic, alunitic and propylitic (Sinclair, 2004). At the same time, iron oxide minerals are developing over many of the porphyry and epithermal deposits due to oxidation sulfide minerals.

In this study, we have processed Enhanced Thematic Mapper Plus (ETM+) data from Landsat 7, which was launched in April 1999. Bands 1 to 7 are in blue, green, red, near infrared and shortwave infrared with 30 m ground resolution. The thermal infrared band (band 6) of ETM+ has a ground resolution of 60 m. The panchromatic 8 band has a resolution of 15 m (Gupta, 2003). The TM bands spectral ranges are shown in Table 1.

In addition to ETM+ data analysis, interpretation of airborne geophysics data (magnetometery and radiometry) can also be used for porphyry and epithermal systems exploration (Dickson *et al*., 1996; Ranjbar *et al*., 2001; Ranjbar and Honarmand, 2004).

Table 1: TM spectral passband

Band No.	Band pass (spectral range) (μm)	Spatial resolution (m)
1	0.45-0.52	30
2	0.52-0.60	30
3	0.63-0.69	30
4	0.75-0.90	30
5	1.55-1.75	30
6	10.40-12.50	60
7	2.08-2.35	30
8	0.52-0.90	15

Corresponding Author: A. Malekzadeh Shafaroudi, Research Center for Ore Deposit of Eastern Iran, Ferdowsi University of Mashhad, P.O. Box 91775-1436, Mashhad, Iran

The aim of this study is to process ETM$^+$ images using different techniques and analyze airborne geophysics data (magnetometry and radiometry) for locating porphyry copper and epithermal gold prospects in Eastern Iran. The study area is located 70 km Southwest of Birjand city, the center of South Khorasan province in Eastern Iran. The climate in the district is arid to semi-arid and vegetation is very weakly developed, optimizing the possibility for observation of bedrock alteration from satellite imagery.

GEOLOGIC SETTING

The investigated area is situated within the eastern part of the so-called Lut block of eastern Iran. Eastern Iran and particularly the Lut block, has a great potential for different types of mineralization as a result of its past subduction zone tectonic setting, which lead to extensive magmatic activity forming igneous rocks different geochemical compositions. The Lut block is characterized by extensive exposure Tertiary volcanic and subvolcanic rocks formed due to subduction prior to the collision of the Arabian and Asian plates (Camp and Griffis, 1982; Tirrul *et al*., 1983; Berberian *et al*., 1999).

Most of the study area is covered by upper Eocene-Oligocene altered volcanic rocks including andesite, dacite, tuff and ignimbrite. These rocks are intruded by porphyritic felsic to intermediate intrusive rocks consisting of monzonite, diorite and microgranodiorite porphyry stocks. Sedimentary rocks in this area consist of conglomerates, minor middle Eocene to upper Eocene tuffaceous marls in the southeastern to eastern area and Quaternary sediments (Fig. 1).

Different types of metal ore bodies, such as porphyry Cu, Cu-Au-Fe-oxide (IOCG), vein type, massive sulfide, Au-epithermal, intrusion-related gold systems and Sn-W-skarns and also non-metal deposits (bentonite, kaoline) have already been documented in the Lut block. Four porphyry copper and epithermal gold prospects in this region (Fig. 1) are named Maherabad, Sheikhabad, Khopik and Hanich. Each is associated with a well- developed area of hydrothermal alteration.

Maherabad prospect area is a Cu-Au porphyry system. Maherabad prospect is dominated by subvlcanic intrusive rocks such as monzonite and diorite porphyry stocks that intruded into upper Eocene-Oligocene volcanic rocks (andesite, tuff and dacite) (Fig. 1). Quartz-Sericite-Pyrite (QSP), argillic and propylitic alteration are most common in the area. Alteration minerals include quartz, sericite, carbonate, chlorite, epidote and clay minerals. Intense quartz stockwork associated with pyrite and minor chalcopyrite as well as oxidized zone minerals such as malachaite, iron oxides, clay minerals and copper wad is associated with mineralization in this region. Cu (300 ppm to up to 1 wt %) and Au (200 to up to 500 ppb) anomalies are coincident with the alteration zones.

Sheikhabad prospect consists of argillic, alunitization, sericitic and silicified zones which are best developed within upper Eocene-Oligocene andesite, tuff, ignimbrite and dacite that are partly intruded by diorite porphyry dikes (Fig. 1). Dissiminated minor pyrite and secondary iron oxides are present in this region. Au and Cu anomalies are coincident. This area can be a high-sulfidation epithermal gold system, which formed above a Cu-Au porphyry deposit.

Khopik prospect area is a Cu-Au porphyry deposit. The geology of the Khopik prospect area is partly characterized by hornblend-monzonite porphyry associated with potassic alteration (secondary biotite+ magnetite+quartz±chlorite±K-feldspar±calcite), which is in faulted contact with volcanic rocks such as andesite and dacite. Most of this area is dominantly volcanic rocks (Fig. 1). Other hydrothermal alteration includes sericitic, argillic, tourmalization and propylitic zones that have been telescoped with potassic alteration by faulting activity. Stockwork, open space filling and dissiminated mineralization are recognized. Pyrite and magnetite as well as minor chalcopyrite are common in this area. Oxidized zone consists of malachaite and iron oxides. Geochemical data show that Cu (300 ppm to up to 1.5%) and Au (150 to up to 2000 ppb) concentration are coincident.

Hanich prospect area is similar to low-sulfidation epithermal systems. The rocks are dominantly altered andesite and dacite (Fig. 1). Argillization, sericitization and silicification are common hydrothermal alteration in this area. Mineralization is not seen at surface.

MATERIALS AND METHODS

In this study, we have analyzed ETM$^+$ data for the identification of hydrothermal alteration. Processing procedures were done by ENVI 4.0 software. The investigated area is within an approximately 374 km^2 subset of the ETM$^+$ scene (WRS- Path =159, Raw = 038, Acquisition data 2002/08/06). Bands1, 2, 3, 4, 5, 7 and 8 have been used for this study. The images have been corrected by using control points from topographic sheets. Both subscenes are jointed together to form a single image. Different image processing techniques such as false color composite images, ratio images, color composite ratio image, Principal Component Image Analysis (PCA), Intensity-Hue-Saturation (IHS) transformation, filtering, supervised classification and unsupervised classification are normally used for

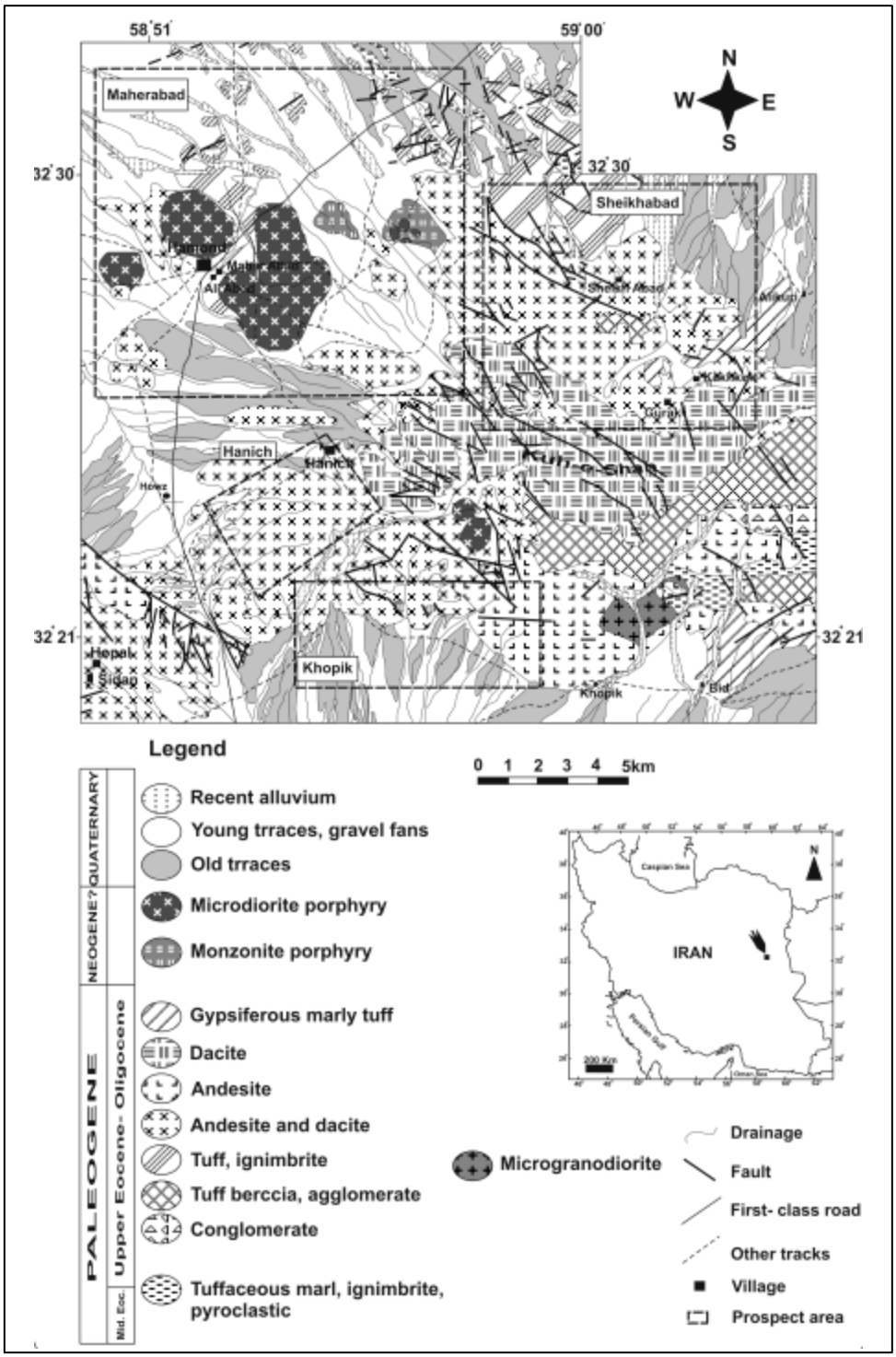

Fig. 1: Simplified regional geological map of study area modified after the Sar-e-chah-e-shur map (Vassigh and Soheili, 1975), Mokhtaran map (Movahhed-avval and Emami, 1978) and Khosf map (Eftekharnezhad *et al.*, 1989). The location of four known prospect areas is shown

delineating the favorable areas for further exploration. In this study, three different processing techniques have been used for detection of porphyry Cu-Au and epithermal Au deposits in eastern Iran. These are as follow: (1) false color composite, (2) color composite ratio images and (3) Principal Component Analysis (PCA).

The airborne geophysics data we have used in this research involved magnetometry and radiometry done over the South Khorasan province in 2005 by Geological Survey of Iran (GSI). The aim of this survey was exploration for mineral deposits in eastern Iran. The flight line spacing was chosen at 200 m. The elevation of flight and elevation of sensor were 65 and 30 m, respectively.

The obtained results from ETM$^+$ images processing and their integration with airborne geophysics data have been confirmed by on the ground field geology such as geological, alteration and mineralization mapping, geochemical explorations and magnetic susceptibility measurements in the district.

RESULTS AND DISCUSSION

ETM$^+$ data analysis: Reflectance spectra of some common clay minerals, alunite and iron oxides are shown in Fig. 2 and 3. TM band 7 (2.1- 2.4 μm) absorption features detect mainly clay and sheet silicates, which contain Al-OH- and Mg-OH- bearing minerals and hydroxides in the alteration zone, due to molecular vibrational processes becoming very prominent (Fig. 2). These minerals have higher reflectance values within TM band 5 (1.55-1.75 μm) (Fig. 2).

Iron oxides, which contain Fe-OH bearing minerals in the gossan zone, have higher absorption within ETM$^+$ band 1 (0.45-0.52 μm) and higher reflectance within TM band 3 (0.63-0.69 μm) (Fig. 3). These bands provide a useful tool for detection of alteration minerals assemblage in different image processing techniques described below:

False color composite image: Several false color composite images were produced for enhancing the identification of hydrothermal alteration in the study area. Figure 4 is a false color composite image of TM bands 7-5-4 shown in red, green and blue respectively. Sericitic and argillic alteration zones in Maherabad, Sheikhabad, Khopik and Hanich prospect areas can be distinguished by a white-green color. The prophylitic zones were recognized by brown color. In Khopik area, this is in brown-orange color due to intense chloritization and epidotization. Another small area of alteration is detected in southeastern region, north of Bid village, within andesite and tuff. This can to be a new prospect area for further exploration. Vegetation has a higher reflectance in

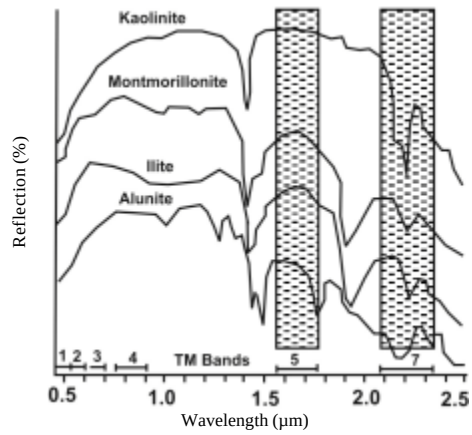

Fig. 2: Reflectance spectra of some common clay minerals (after Sabins, 1997)

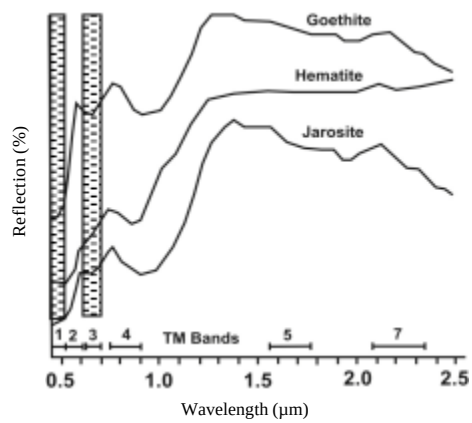

Fig. 3: Spectral reflectance curves for jarosite, hematite and goetite (after Sabins, 1997)

TM band 4 (0.75-0.90 μm). Vegetation locations were shown by blue color in the study area. The color composite RGB: 754 did not show very good results for lithologic discrimination. The Kuh-e-Shah dacite and volcanic rocks south of it were recognized by dark green and violate color respectively. Microgranodiorite unit in the Southeastern part of district were characterized by white color, whereas tuff unit in northwestern part of the area has a similar color. Volcanic rocks in the northern part of the study area were detected by violate color that are similar to these rocks in south and southeastern area (Fig. 4).

Color composite ratio images: Ratio techniques are a highly effective means of minimizing brightness variations owing to the topographic slope and changes in albedo. In this technique, bands with high reflectance are divided by

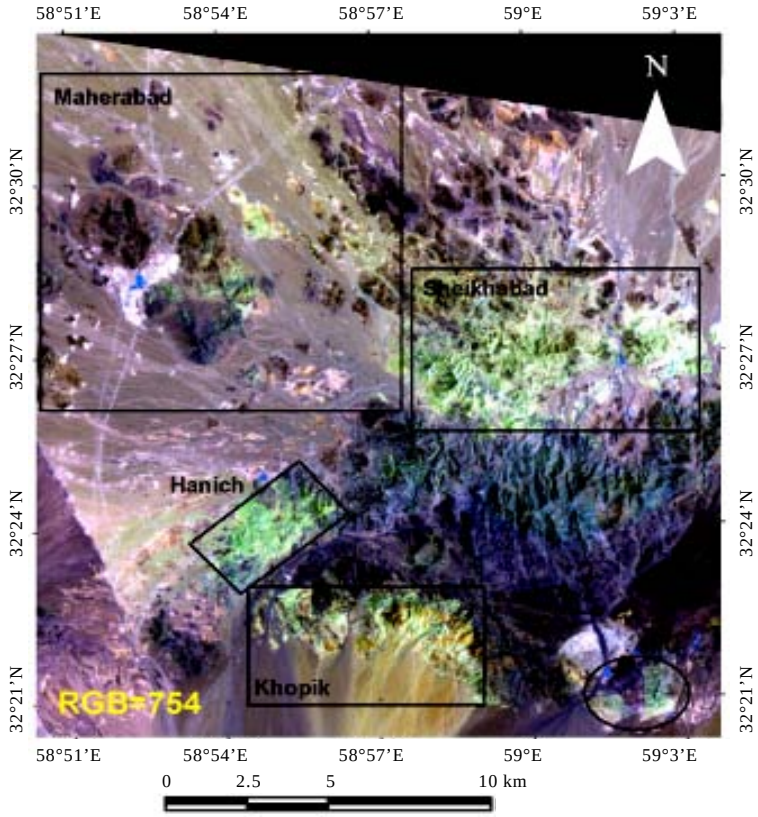

Fig. 4: Red-Green-Blue color composite of bands 7, 5 and 4

bands with high absorption. Therefore a ratio of band 5/ band 7 would yield very high values for altered zones comprising dominantly hydroxyl- bearing minerals. This characteristic of phyllosilicates has been used in numerous mineral exploration investigations. With the same technique, iron oxide minerals can be detected by the band 3/band 1 ratio (Sabins, 1999).

Color composite ratio images are produced by combining three ratio images in red, green and blue. An advantage of the color composite ratio images is that it combines the distribution patterns of both iron minerals and hydrothermal clays. A disadvantage is that the color patterns are not as distinct as in the individual density-sliced images (Sabins, 1999).

More than 20 color composite ratio images have been produced for target location. Two of these are presented here. In the RGB: 5/7, 5/4, 3/1 (Fig. 5), the area in white, bright blue- green, pink and yellow shows a response of band 5 and 7 (Al-OH- bearing minerals) and band 3 and 1 (Fe-OH- bearing minerals). The four prospect areas can be detected by this technique. The small altered region to the east of Khopik prospect area can also be distinguished by white- pink pixels too. Propylitic alteration can be recognized by yellow- green color in this area. Vegetation is detected by red color (Fig. 5). Discrimination of different rock unites is similar to previous technique shown Fig. 4.

In bright red is Kuh-e-Shah dacite, in violate to green- violate is unaltered volcanic rocks, in blue- white is microgranodiorite unit and in blue is tuff unit of northwestern study area (Fig. 5).

The band ratio RGB: 5/7, 2/7, 7/4 shows hydrothermal alteration in pink, blue, dark blue and yellow colors. Five altered areas have been shown in Fig. 6. Vegetation is in orange. Kuh-e-Shah dacite and volcanic rocks are in yellow- orange and yellow- green color, respectively. The tuff unit and propylithic zone do not differ in color and both are in dark blue (Fig. 6).

Principal Component Analysis (PCA): The Principal Component Analysis (PCA) is widely used for alteration mapping in metallogenic provinces (Kaufman, 1988; Crosta and Moore, 1989; Bennet *et al.*, 1993; Rutz-Armenta and Prol-Ledesma, 1998; Abrams *et al.*, 1983; Tangestani and Moore, 2002; Ranjbar *et al.*, 2004; Jing and Panahi, 2006).

This technique is a multivariate statistical technique that selects uncorrelated linear combinations (eigenvector loadings) of variables in such a way that each

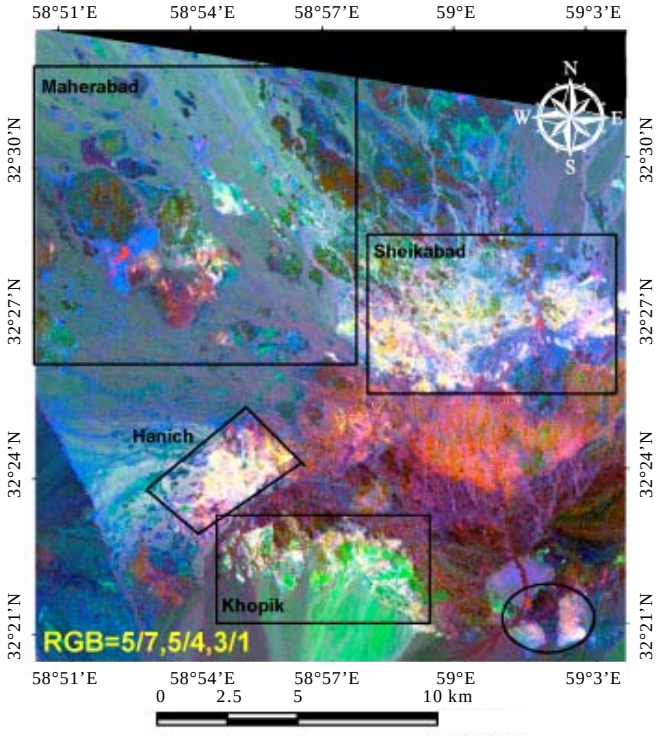

Fig. 5: Red-green-blue color composite ratio image of 5/7, 5/4, 3/1

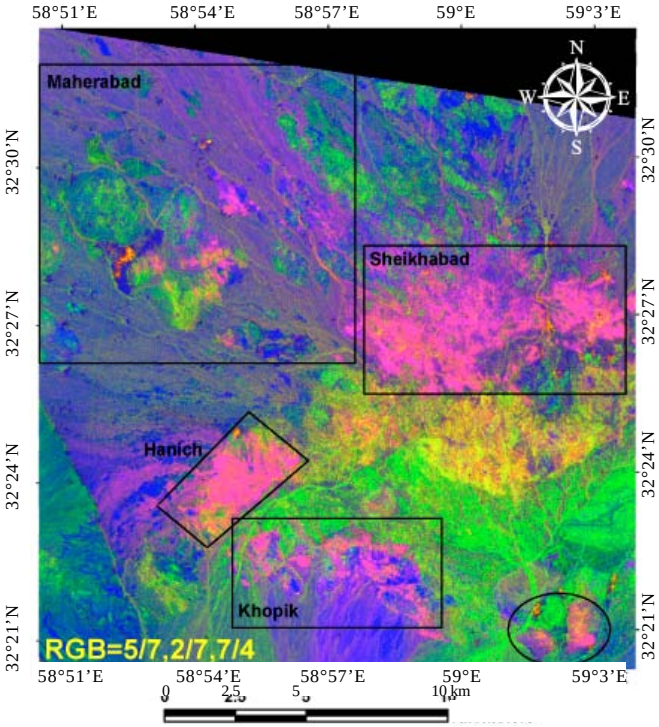

Fig. 6: Red-green-blue color composite ratio image of 5/7, 2/7, 7/4

Table 2A: General statistics for 6 bands

	Bands					
	1	2	3	4	5	7
Maximum	136.00	174.00	148.00	184.00	136.00	122.00
Mean	66.21	76.12	68.45	89.69	70.62	72.46
SD	22.31	26.22	21.12	27.60	21.01	20.77

Table 2B: Correlation matrix for 6 bands

	Bands					
Bands	1	2	3	4	5	7
1	1.00					
2	0.97	1.00				
3	0.95	0.93	1.00			
4	0.95	0.93	0.99	1.00		
5	0.93	0.91	0.98	0.99	1.00	
7	0.89	0.86	0.95	0.97	0.98	1.00

Table 2C: Principal components for 6 bands

	PC					
	1	2	3	4	5	6
Band 1	0.38	0.38	0.55	0.59	0.19	0.01
Band 2	0.45	0.66	-0.11	-0.57	-0.12	0.01
Band 3	0.37	-0.11	-0.56	0.11	0.71	0.00
Band 4	0.49	-0.22	-0.32	0.32	-0.60	0.35
Band 5	0.37	-0.30	0.07	-0.06	-0.17	-0.85
Band 7	0.35	-0.50	0.49	-0.43	0.19	0.37
Covariance eigenvalue	3133.02	106.10	13.18	9.08	4.03	1.44
Variance (%)	95.90	3.24	0.40	0.27	0.12	0.04

successively extracted linear combination, or Principal Component (PC), has a smaller variance (Singh and Harrison, 1985).

Three PCA techniques have been used for satellite images processing: (1) standard PCA on six bands of Landsat, (2) Crosta technique on four or six bands and 3) selective PCA on two or three bands.

In this study, the general statistics and principal component eigenvectors and eigenvalues for six, four and three bands have been calculated in different ways. More than 20 different alteration maps of this area have been produced by these PCA techniques and their color compositions. The best processed images have been selected and are described below.

The statistics and principal component transformation (eigenvectors and eigenvalues) are described in Table 2A-C, using six ETM^+ bands as input bands (bands 1, 2, 3, 4, 5 and 7). It is observed the PC1 does not contain spectral features relevant in this analysis as it is a combination of all bands. This component contains 95.9% of the variance of the 6 bands (Table 2C). The PC1 gives information mainly on albedo and topography. Vegetation should be enhanced in PC5 as this PC has higher with negative sign (-0.60) loading of band 4. The PC6 has higher loadings of band 5 (-0.85). This PC should detect the hydroxyl minerals in dark pixels because of negative contributions of band 5 and positive contributions of band 7 (0.37). The PC5 has a higher positive loading of band 3 (0.71). This PC should represent iron oxides in bright pixels because of positive contributions of band 3 and band 1 (Table 2C). Although the principal component eigenvectors and eigenvalues indicate important of PC5 and PC6 for alteration detection, these PC images have not clearly shown the location of four prospect areas.

The PC4 image clearly detects the location of alteration zones in dark pixels. In order to show the areas with hydroxyl minerals in bright pixels an inverse of this PC is obtained by using Eq. 1.

$$PC4 = -0.59\ (\text{band } 1)+0.57\ (\text{band } 2)-0.11\ (\text{band } 3)-0.32\ (\text{band } 4)+0.06\ (\text{band}5)+0.43\ (\text{band } 7) \quad (1)$$

Color composition PC images are also useful technique for hydrothermal alteration mapping (Conradsen and Harpoth, 1984; Ranjbar *et al*., 2004; Roustaei *et al*., 2006). This technique is produced by combining three PC images in red, green and blue. Color composition of PC3, PC2 and PC4 (using 7 bands as input bands) in red-green-blue is shown in Fig. 7. Sericitic and argillic alteration have been characterized by green color. Propylitic zone is in yellow- orange to pink. As with the previous techniques, a fifth altered area is detected by green color. Vegetation can be detected by dark green color (Fig. 7).

Discrimination of different rock units is shown: in green-brown color is Kuh-e-Shah dacite, in dark red to violate are volcanic rocks, in dark blue is micrograndiorite and in bright blue is the tuff unit. Plutonic rocks near the villages in Maherabad area are the same color as volcanic rocks (Fig. 7).

Crosta technique is also used for features oriented principal components selection. Through the analysis of the eigenvector values it allows identification of the principal components that contain spectra information about specific minerals, as well as the contribution of each of the original bands to the components in relation with spectral response of the materials of interest. This technique can be applied on four and six selected bands on TM data (Crosta and Moore, 1989; Rutz-Armenta and Prol- Ledesma, 1998). Crosta technique is commonly used on Bands 1, 3, 4 and 5 for enhancing iron oxides and bands 1, 4, 5 and 7 for detection hydroxyl minerals. Although the Crosta method is very useful for the alteration mapping; nevertheless, there are areas which are altered but are not enhanced by this technique (Ranjbar and Honarmand, 2004). Crosta technique has been used for alteration mapping in study area but this technique proved not to be useful.

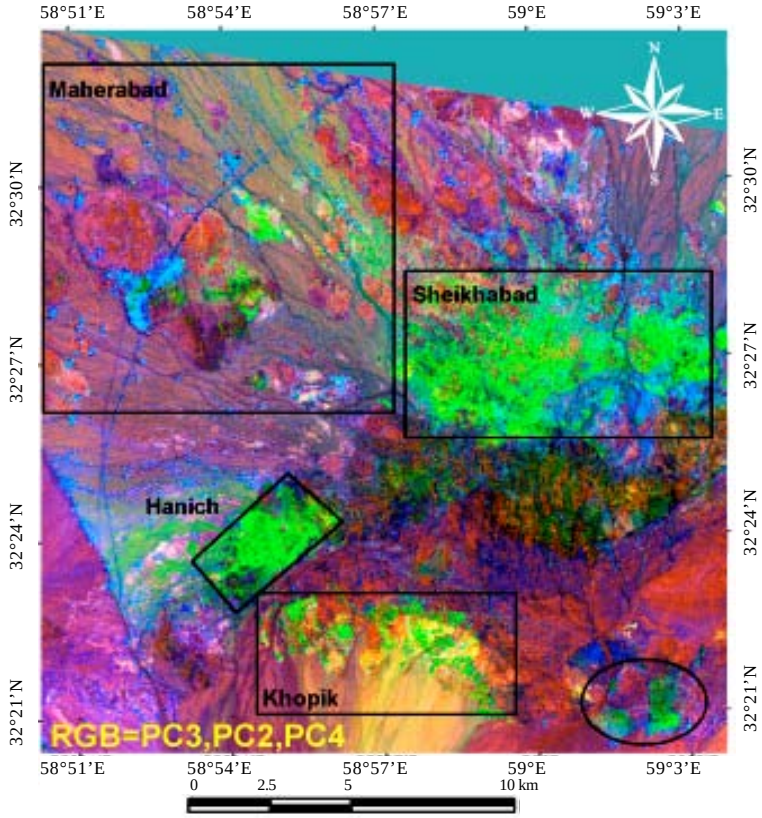

Fig. 7: Red-green-blue color composite image of PC3, PC2, PC4 (using 7 bands as input bands)

Table 3A- General statistics for 3 bands

	Band 1	Band 4	Band 5
Maximum	174.00	148.00	122.00
Mean	76.12	68.45	72.46
SD	26.22	21.12	20.77

Table 3B: Correlation matrix for 3 bands

Bands	Band 1	Band 4	Band 5
1	1.00		
4	0.93	1.00	
5	0.86	0.95	1.00

Table 3C: Principal components for 3 bands

	PC1	PC2	PC3
Band 1	0.66	0.54	0.51
Band 4	0.69	-0.19	-0.68
Band 5	-0.27	0.81	-0.51
Covariance eigenvalue	1479.96	76.07	9.39
Variance (%)	94.54	4.85	0.59

Table 4A: General Statistics for 3 bands

	Band 1	Band 4	Band 5
Maximum	136.00	174.00	122.00
Mean	66.21	76.12	72.46
SD	22.31	26.22	20.77

Table 4B: Correlation matrix for 3 bands

Bands	Band 1	Band 5	Band 7
1	1.00		
5	0.97	1.00	
7	0.89	0.86	1.00

Table 4C: Principal components for 3 bands

	PC1	PC2	PC3
Band 1	0.56	0.65	0.49
Band 5	0.17	0.48	-0.85
Band 7	-0.80	0.57	0.15
Covariance eigenvalue	1532.02	75.40	9.61
Variance (%)	94.74	4.66	0.59

The selected principal component analysis on three bands has also been applied in study area. The statistics and PC eigenvectors and eigenvalues have been calculated in Table 3A-C and 4A-C, using bands 1, 4 and 5 and bands 1, 5 and 7 as input bands, respectively.

Table 3C shows that vegetation should be enhanced in PC3 because of higher loadings of band 4 (-0.68). PC2 has higher loadings of band 5 (0.51). This PC should detect hydroxyl minerals with bright pixel due to positive contributions of band 5.

Table 4C shows that hydroxyl minerals should be enhanced in PC3 because of higher loadings of band 5 (-0.85). Hydroxyl minerals can be detected in dark pixels due to the negative contribution of band 5 and positive

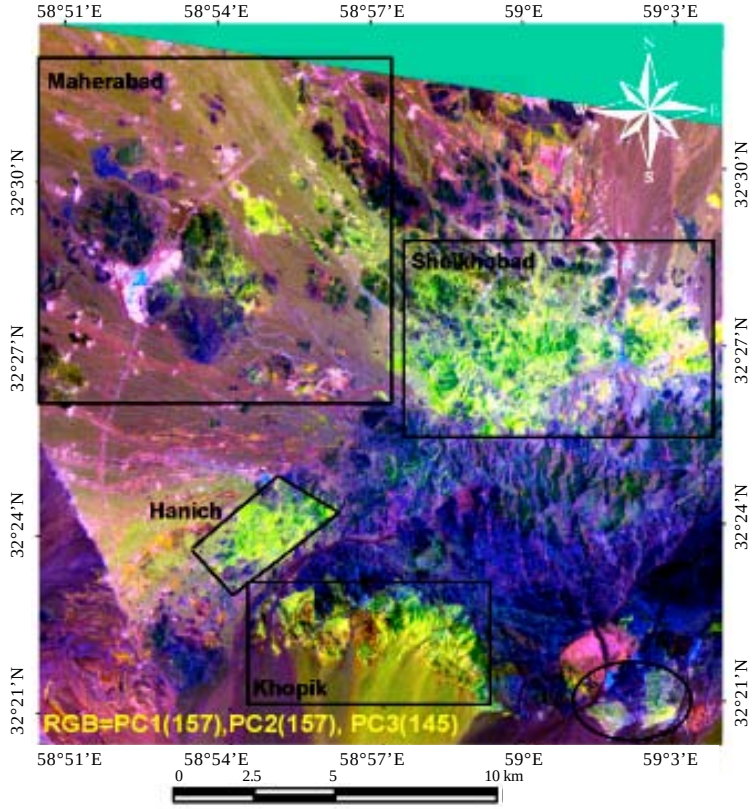

Fig. 8: RGB color composite image of PC1 (157), PC2 (157), PC3 (145)

contribution of band 7 (0.15). In order to show hydroxyl minerals in bright pixels an inverse of this PC is obtained by using Eq. 2. PC2 can recognize hydroxyl minerals in bright pixels too (Table 4C).

$$PC3 = -0.49\ (\text{band } 1) + 0.85\ (\text{band } 5) - 0.15\ (\text{band } 7) \quad (2)$$

Color composition PC images have been combined by PC1 (157), PC2 (157) and PC3 (145) in red, green and blue, respectively (Fig. 8). The areas in green, yellow and white colors are sericitic and argyllic alterations. Propylitic zones can be detected by darker green and brown color. In addition to the four known prospect areas, a fifth altered region was also recognized by this technique. Vegetation is enhanced in blue color. Discrimination of Kuh-e-Shah dacite and volcanic rocks is not very good and both are in dark blue- violate color. Microgranodiorite unit (southeast of area) is in pink. Tuff unit is in white too (Fig. 8).

Airborne geophysics data analysis: Airborne geophysics data (radiometry and magnetometry) is another useful tool for porphyry copper and epithermal gold systems exploration.

Behn *et al.* (2001) argued that high- resolution aeromagnetic data from northern Chile shows that of porphyry copper deposits coincide with magnetite anomalies, which most likely reflect loci of mafic intrusions in mid to deep crustal level.

Ranjbar *et al.* (2001) and Ranjbar and Honarmand (2004) have worked on a airborne geophysics data and concluded that the porphyry copper deposits in the Kerman region are associated with a distinct magnetic lows relative to the host rocks. Their potassium is high and resistivity is low.

Airborne magnetometry studies in Infiernillo porphyry deposit, Argentina, have shown a positive anomaly approximately coincident with the potassic zone, surrounded by a relatively low magnetic intensity halo suggesting magnetic destruction, features typical of the phyllic zone (Tommaso and Rubinstein, 2007).

Dickson *et al.* (1996) have shown, in Kerman province that elevated potassium in the sericite zone is often observed around the mineralization areas. Also acid sulfate conditions resulting from weathering of near surface sulfides can result in Th mobilization from host rocks and Th can precipitate with iron in gossan. Similar

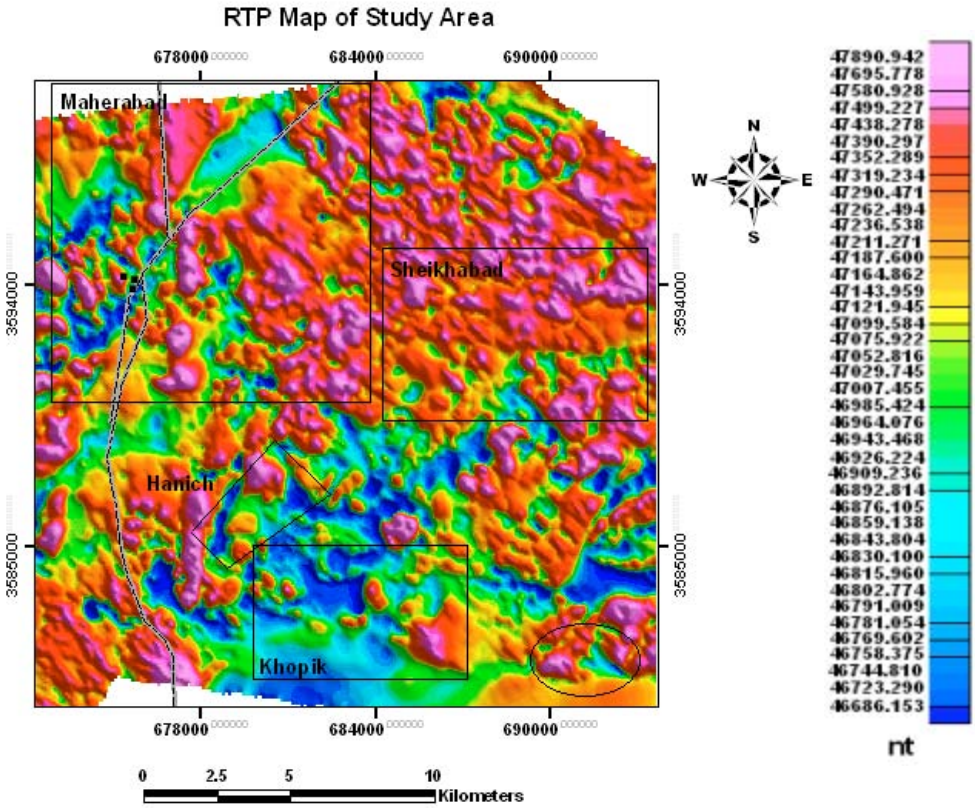

Fig. 9: RTP map of study area (GSI, 2005)

results have been obtained over the Darrehzar prospect area, near the Sarcheshmeh porphyry deposit. The higher K and Th counts over the altered zone are due to the presence of abundant sericite, clay and K-feldspar minerals (Ranjbar *et al*., 2001).

Figure 9 shows Reduced to Pole Magnetic (RTP) map of the study area that has been produced by the Geological Survey of Iran (2005). Field intensity and shape of anomaly were changed by magnetic dipoles and their location relative to the Earth magnetic field and strike of flight lines. Therefore using the RTP filter these effects are omitted and the magnetic anomaly is returned to its true situation. The maximum and minimum fields in the RTP map are 47890.924 and 46686.153 nt, respectively (Fig. 9).

The magnetic anomaly is related to the erosion level of porphyry and epithermal deposits, the type of alteration and mineral assemblage observed in surface and the intensity of alteration and amount of magnetite destruction. Increase of erosion-level is indicated by outcrops of magnetite-type granitoid rocks hosting mineralization and the presence of potassic alteration associated with magnetite (particularly in Cu-Au porphyry deposit). Types of alteration and minerals assemblage influence magnetic intensity, as potassic and propylitic zones occasionally have high magnetite content and sericitic and argillic zones don't have magnetite due to its destruction.

In the study area, the high magnetic anomaly is related to magnetite-series intrusive rocks that commonly host alteration and mineralization at both the surface and at depth (Fig. 9). Magnetic susceptibility measurements of volcanic-plutonic rocks (80×10^{-5} to $>5000\times10^{-5}$ SI) confirmed this idea. In this manner magnetite veins are occasionally present in propylitic and potassic zones. The area with a relatively low magnetic intensity suggested magnetic destruction in other types of alteration zone (Fig. 9).

Figure 10 shows a ternary radiometry map of the area. Three radioelement concentrations are shown: potassium as red, uranium as blue and thorium as green. On the map, blue areas are relatively high in uranium, red areas are relatively high in potassium and green areas are relatively high in thorium. The intensity of each color is proportional to the concentration. White areas have very low radioelement concentration normally due to overburden covering the bedrock (Fig. 10).

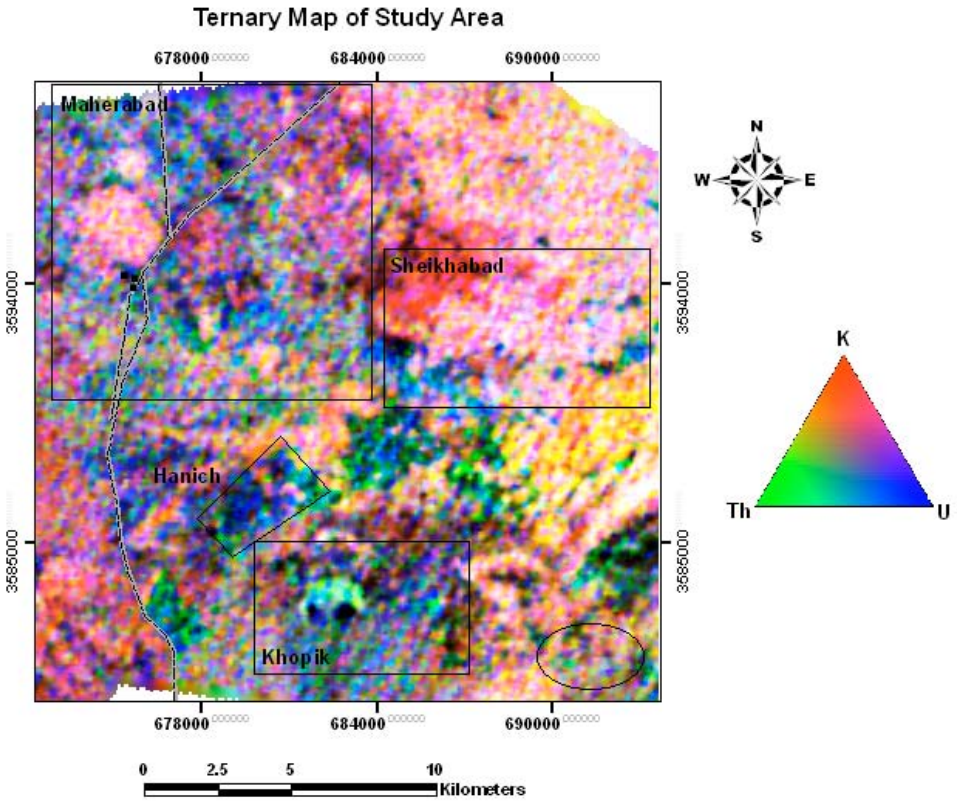

Fig. 10: Ternary map of study area (GSI, 2005)

The high potassium and uranium counts over the prospect areas reflect the presence of sericite, K- feldspar and clay minerals. The high thorium count can be implied to be in gossan zone in which Th has been precipitated along with iron (Fig. 10).

CONCLUSION

The Lut block has a great potential for different types of mineralization, particularly porphyry copper and epithermal gold deposits, as result of its suitable subduction zone tectonic setting resulting in the presence of calcalkaline subvolcanic rocks. Maherabad, Sheikhabad, Khopik and Hanich prospect areas are the best documents for this claim. Eastern Iran can potentially become the second important porphyry copper belt in Iran after Urumieh-Dokhtar zone.

ETM$^+$ images processing is a valuable technique for delineating favorable areas for further exploration. This technique works very well in eastern Iran due to low precipitation causing very minor soil development and the small amount vegetation and therefore good rock exposure. Getting access to the most of the region due to lack of roads cause exploration to be expensive and time consuming. ETM$^+$ data analysis for detection and reconnaissance mapping of iron oxides and hydroxyl minerals zones in areas with low vegetation cover can to be an excellent low-cost alternative method of exploration. Integration of both satellite images processing and airborne geophysics data can obtain better results.

In this study, different image processing methods consists of false color composite images, color composite ratio images and different techniques of principal component analysis and their color compositions have been used. All of these techniques clearly show the four known prospect areas in the study area, but color composition selective images may be the most reliable method for enhancing the areas with hydrothermal alteration. In addition to the four known porphyry-epithermal prospect areas, a fifth previously unknown small altered area has also been detected in southeastern district.

Airborne magnetometry data shows high concentrations of magnetic over the most of the study area reflected of magnetic-series granitoid rocks related to mineralization or propylitic/potassic zone with magnetite

veins. Low magnetic areas reflect magnetic destruction in other types of alteration zone. The high K and U counts have resulted from the presence of sericite, clay minerals and K-feldspar. The high thorium count occurs in gossan zones in which Th has been precipitated with iron.

REFERENCES

Abrams, M.J., R.P. Ashley, L.C. Brown, A.F.H. Goetz and A.B. Kahle, 1977. Mapping of hydrothermal alteration in the Cuprite mining district, Nevada, using aircraft scanning images for the spectral region 0.46 to 2.36 mm. Geology, 5: 713-718.

Abrams, M.J., L. Brown, R. Lepley and P. Sadowski, 1983. Remote sensing for porphyry copper deposits in Southern Arizona. Econ. Geol., 78: 591-604.

Amos, B.J. and D. Greenbaum, 1989. Alteration detection using TM imagery, the effects of supergene weathering in an arid climate. Int. J. Remote Sens., 10: 515-527.

Behn, G., F. Camus and P. Carrasco, 2001. Aeromagnetic signature of porphyry copper systems in northern Chile and its geologic implications. Econ. Geol., 96: 239-248.

Bennet, S.A., W.W. Atkinson and F.A. Kruse, 1993. Use of thematic mapper imagery to identify mineralization in the santa teresa district, Sonara, Mexico. Int. Geol. Rev., 35: 1009-1029.

Berberian, M., J.A. Jackson, M. Qorashi, M.M. Khatib, K. Priestley, M. Talebian and M. Ghafuri-Ashtiani, 1999. The 1997 may 10 Zirkuh (Qaenat) earthquake (Mw 7.2): Faulting along the Sistan suture zone of eastern Iran. Geophys. J. Int., 136: 671-694.

Buckingham, W.F. and S.E. Sommer, 1983. Mineralogical characterization of rock surfaces formed by hydrothermal alteration and weathering-application to remote sensing. Econ. Geol., 78: 664-674.

Camp, V. and R. Griffis, 1982. Character, genesis and tectonic setting of igneous rocks in the Sistan suture zone, eastern Iran. Lithous, 15: 221-239.

Chen, X., T.A. Warner and D.J. Campagna, 2007. Integration visible, near-infrared and short-wave infrared hyperspectral and multispectral thermal imagery for geological mapping at Cuprit, Nevada. Remote Sens. Environ., 110: 344-356.

Conradsen, K. and O. Harpoth, 1984. Use of Landsat multispectral scanner data for detection and reconnaissance mapping of iron oxide staining in mineral exploration, central east Greenland. Econ. Geol., 79: 1229-1244.

Crosta, A. and J.M.M. Moore, 1989. Enhancement of landsat thematic mapper imagery for residual soil mapping in SW Minais Gerais State, Brazil: A prospecting case history in Greenstone belt terrain. Proceedings of the Seventh ERIM Thematic Conference: Remote Sensing for Exploration Geology, October 2-6, Calgary, Alberta, Canada, pp: 1173-1187.

Dickson, B.L., S.J. Fraser and A. Kinsey-Henderson, 1996. Interpreting aerial gamma-ray surveys utilizing geomorphological and weathering models. J. Geochemical Explorat., 57: 75-88.

Drury, S.A. and G.A. Hunt, 1989. Geological uses of remotely-sensed reflected and emitted data of lateralized Archean terrain in Western Australia. Int. J. Remote Sens., 10: 475-497.

Goetz, A.F.H., B.N. Rock and L.C. Rowan, 1983. Remote sensing for exploration: An overview. Econ. Geol., 78: 573-590.

Gupta, R.P., 2003. Remote Sensing Geology. 2nd Edn., Springer Verlag, Heidelberg, pp: 566.

Jing, Q.C.L. and A. Panahi, 2006. Principal component analysis with optimum order sample correlation coefficient for image enhancement. Int. J. Remote Sens., 27: 3387-3401.

Kaufman, H., 1988. Mineral exploration along the Agaba-Levant structure by use of TM-data concepts, processing and results. Int. J. Remote Sens., 9: 1639-1658.

Ramadan, T., A. Yahia, Sh. Fawzy and S. Gad, 2001. Exploration for the mineralized granites in Arabo-Nubian shield, using orbital remote sensing. GSA Annual Meeting, November 5-8, 2001, Boston, Massachusetts. http://gsa.confex.com/gsa/2001AM/finalprogram/abstract_22919.htm.

Ranjbar, H., H. Hassanzadeh, M. Torbati and O. Ilaghi, 2001. Integration and analysis of airborne geophysical data of the Darrehzar area, Kerman Province, Iran, using principal component analysis. J. Applied Geophys., 48: 33-41.

Ranjbar, H. and M. Honarmand, 2004. Integration and analysis of airborne geophysical and ETM+ data for exploration of porphyry type deposits in the central Iranian volcanic belt using fuzzy classification. Int. J. Remote Sens., 25: 4729-4741.

Ranjbar, H., M. Honarmand and Z. Moezifar, 2004. Application of the crosta technique for porphyry copper alteration mapping, using ETM^+ data in the southern part of the Iranian volcanic sedimentary belt. J. Asian Earth Sci., 24: 237-243.

Roustaei, M., M. Dehghani, J. Gingerich and C. Durocher, 2006. Mineral potential mapping in Khoy-Oshnavieh area of NW Iran, using Landsat ETM+ and ASTER images. J. Geol. Soc. Iran, 1: 43-51.

Rowan, L.C., S.G. Hook, A.J. Abrams and J.C. Mars, 2003. Mapping hydrothermally altered rocks at Cuprite, Nevada, using the advanced spaceborne thermal emission and reflection radimeter (ASTER), a new satellite-imaging system. Econ. Geol., 98: 1019-1027.

Rutz-Armenta, J.R. and R.M. Prol-Ledesma, 1998. Techniques for enhancing the spectral response of hydrothermal alteration minerals in Thematic Mapper images of Central Mexico. Int. J. Remote Sens., 19: 1981-2000.

Sabins, F.F., 1997. Remote Sensing, Principles and Interpretation. 3rd Edn., Freeman, New York.

Sabins F.F., 1999. Remote sensing for mineral exploration. Ore Geol. Rev., 14: 157-183.

Sinclair W.D., 2004. Porphyry deposits. Geological Survey of Canada, pp: 14. http://gsc.nrcan.gc.ca/mindep/synth_dep/porph/pdf/deposit_synthesis.porphyry.sinclair.pdf.

Singh, A. and A. Harrison, 1985. Standardized principal components. Int. J. Remote Sens., 6: 883-896.

Swayze, G.A., R.N. Clark, A.F.H. Goetz, K.E. Livo and S.S. Sutley, 1998. Using imaging spectroscopy to better understand the hydrothermal and tectonic history of the Cuprite mining district, Nevada. Summaries of the 7th JPL Airborne Earth Science Workshop: Vol. 1, January 12-16, Jet Propulsion Laboratory, Pasadena, California, pp: 383-384.

Tangestani, M.H. and F. Moore, 2002. Porphyry copper alteration mapping in the Meiduk area, Iran. Int. J. Remote Sens., 23: 4815-4825.

Tirrul, R., I.R. Bell, R.J. Griffis and V.E. Camp, 1983. The Sistan suture zone of eastern iran, Geol. Soc. Am. Bull., 94: 134-156.

Tommaso, I.D. and N. Rubinstein, 2007. Hydrothermal alteration mapping using ASTER data in the *Infiernillo porphyry* deposit, Argentina. Ore Geol. Rev., 32: 275-290.